Experimental Mechanics (2024) 64:487–500
https://doi.org/10.1007/s11340-024-01047-z

RESEARCH PAPER

Stress Evaluation Through the Layers of a Fibre-Metal Hybrid Composite by IHD: An Experimental Study

J. P. Nobre[1,2] · T. C. Smit[2] · R. Reid[2] · Q. Qhola[2] · T. Wu[3] · T. Niendorf[4]

Received: 23 October 2023 / Accepted: 19 February 2024 / Published online: 5 March 2024

Abstract

Background Incremental hole-drilling (IHD) has shown its importance in the measurement of the residual stress distribution within the layers of composite laminates. However, validation of these results is still an open issue, especially near the interfaces between plies.

Objectives In this context, this study is focused on experimentally verifying its applicability to fibre metal laminates.

Methods Tensile loads are applied to cross-ply GFRP-steel [0/90/steel]s samples. Due to the difference in the mechanical properties of each ply, Classical Lamination Theory (CLT) predicts a distribution of the uniform stress within each layer, with pulse gradients between them. The interfaces act as discontinuous regions between the plies. The experimental determination of such stress variation is challenging and is the focus of this research. A horizontal tensile test device was designed and built for this purpose. A differential method is used to eliminate the effect of the existing residual stresses in the samples, providing a procedure to evaluate the ability of the IHD technique to determine the distribution of stress due to the applied tensile loads only. The experimentally measured strain-depth relaxation curves are compared with those determined numerically using the finite element method (FEM) to simulate the hole-drilling. Both are used as input for the IHD stress calculation method (unit pulse integral method). The distribution of stress through the composite laminate, determined by classical lamination theory (CLT), is used as a reference.

Results Unit pulse integral method results, using the experimental and numerical strain-depth relaxation curves, compare reasonably well with those predicted by CLT, provided that there is no material damage due to high applied loads.

Conclusions IHD seems to be an important measurement technique to determine the distribution of residual stresses in fibre metal laminates and should be further developed for a better assessment of the residual stresses at the interfaces between plies.

Keyword Fibre-metal laminate · Composite laminate · Residual stress · Hole-drilling method

Introduction

Advances in composite technology have allowed significant weight reduction in structural design. Fibre reinforced polymers (FRP) usually present greater strength and stiffness to weight ratios compared to metallic alloys, also providing excellent fatigue behaviour and corrosion resistance [1]. Fibre metal laminates (FML), primarily developed to be used in aerospace structures, are hybrid composite materials consisting of layers of metallic alloys bonded to FRP plies during the autoclave curing process [2]. The use of these two types of materials to form a hybrid composite material enhances its mechanical behaviour by combining the best properties of each constituent [3, 4]. The curing process of FRPs and FMLs always induces residual thermal stresses due to the mismatch in the coefficients of thermal expansion and mechanical properties between the constituents, the polymer cure shrinkage, and other parameters that affect their magnitude and distribution [5]. Curing of the FML is usually followed by a post-stretching process to mitigate the induced residual stresses [1, 2]. The presence of residual stress alters the midrange stress (or mean stress)

✉ J. P. Nobre
joao.nobre@dem.uc.pt

1 Univ Coimbra, CFisUC, Department of Physics, Coimbra, Portugal

2 School of Mechanical, Industrial and Aeronautical Engineering, University of the Witwatersrand, Johannesburg, South Africa

3 Fraunhofer Institute for Ceramic Technologies and Systems, Dresden, Germany

4 Institute of Materials Engineering, University of Kassel, Moenchebergstr. 3, 34125 Kassel, Germany

within materials and, therefore, the stress ratio during cyclic loading. Fatigue strength can either be enhanced or compromised depending on the contribution of residual stress to the stress ratio [6]. The overall material strength may be adversely affected by the introduction of fibre waviness resulting from the presence of residual stresses in FMLs [7]. Moreover, tensile residual stress may initiate microcracks at pre-existing defects, such as voids within FRP plies, irrespective of whether there is any external loading imposed on the laminate [8, 9]. In addition, the use of high performance thermoplastics requires greater processing temperatures compared to thermoset epoxy matrices, for example in GLARE (GLAss REinforced Aluminium [2, 3]) that was successfully used in large parts of the Airbus A-380 fuselage [10]. Therefore, it is a crucial design consideration for residual stresses to be thoroughly understood and quantified in FML components that are used in applications where structural integrity and safety are of high importance. Moreover, as recently stated by Vu et al. [11], at the minimum, reliable experimental methods are needed for the evaluation and verification of the residual stresses predicted using micromechanical models in FRPs. In this context, the incremental hole-drilling (IHD) technique has been demonstrated to be a viable option to experimentally evaluate residual stresses in composite laminates [12–19].

However, beyond the difficulty in calculating residual stresses from the measured strain relaxation during IHD in composite laminates, other issues related to the technique itself remain. Firstly, the thermomechanical effects of friction and plastic deformation in the drilling process generate heat around the hole, which can modify the residual stresses before they are measured. This is particularly true in the case of polymer materials [20]. Secondly, the IHD technique assumes linear elastic material behaviour, but local damage such as delamination can arise due to high residual stresses induced by the stress concentration around the hole. In these materials, the geometric stress concentration factor also depends on the material and ply stacking sequence, and can be greater than that observed in isotropic materials [21].

In this work, all these issues will be simultaneously analysed in a FML. FML samples are subjected to tensile loading, where the applied loads can be finely controlled. In composite laminates subjected to pure tensile loading the stress through the thickness is not uniform as in isotropic materials, but uniformly distributed in each ply with step/pulse gradients at interfaces. Theoretically, the interfaces are discontinuous stress regions where stresses change abruptly, as predicted by Classical Lamination Theory (CLT) [22, 23]. The experimental determination of such stress distributions is attempted in this work, which is a difficult experimental case for IHD. The main goal is to experimentally determine the strain-depth relaxation curves during IHD in "stress free" FML samples subjected to a tensile load. This is a difficult issue, since the samples are not stress free, but are subjected to residual stresses arising from the manufacturing process. However, based on a hybrid experimental-numerical method (HENM) [24], the effect of these initial stresses can be eliminated, allowing the experimental determination of the IHD strain-depth relaxation curves arising only from the applied tensile load and possible cutting effects. Simulation of the hole-drilling process is performed using the finite element method (FEM), considering the same data as in the experimental tests. During the numerical simulation, incremental hole-drilling is simulated by removing the elements from the mesh corresponding to a given depth increment. Numerical strain-depth relaxation curves, arising only from the applied loads, can thereby be determined. The experimental and numerical curves differ only in the possible thermomechanical effects that develop during hole-drilling of the samples. This allows the through-thickness variation in stress distribution in the FML to be compared between the IHD unit pulse integral method and CLT.

The Incremental Hole-Drilling (IHD) Technique and its Stress Calculation Methods

IHD involves stepwise drilling of a small hole in a sample and measuring the surface strain relief around the hole after each incremental depth increase. However, there is no direct relationship between the relieved strain measured at the surface and the residual stress existing at each depth increment. The well-accepted integral method can be used to relate the relieved strain to the residual stresses. This method, proposed by Schajer in its final format in 1988 [25], considers that the strain relief at the surface is the accumulated result of the residual stresses originally existing in the region of each successive increment, along the total hole depth. The residual stresses are considered constant within each depth increment. To completely define the plane stress state at each depth increment, a typical standard three-gauge rosette is commonly used [26]. For isotropic materials [26], the integral method relates strain relaxation measurements and residual stresses through an integral equation that can be solved considering a set of standard calibration coefficients, which are determined by the finite element method, depending only on the increment size, geometry of the hole and rosette used. These coefficients are nearly material independent, and therefore, a standard procedure could be proposed (ASTM E837) [26]. However, since composite laminates are orthotropic and layered in nature there is a full dependency on the material and ply stacking sequence. Additionally, the trigonometric relation that can be used to relate strains and stresses around the hole in the isotropic case is not valid and the stresses cannot be decoupled [15]. In 2014, Akbari et al. [12] extended the pioneering method of Schajer and Yang

[15] to the incremental hole-drilling measurement of non-uniform residual stresses in composite laminates, proposing the fully coupled unit pulse integral method, which can be written mathematically as:

$$\varepsilon_k(i) = \sum_{l=1}^{3} \sum_{j=1}^{i} \sigma_{jl} \cdot C_{ijkl} k, l = 1, 2, 3 \quad 1 \le i \le n, \tag{1}$$

where $\varepsilon_k(i)$ is the relaxed strain measured by strain gauge number k when the hole depth is i increments deep, σ_{jl} corresponds to the residual stress at depth j in the direction of the strain gauge l and C_{ijkl} is the compliance matrix.

Equation (1) considers all three stress and strain directions simultaneously and is valid provided that linear elastic material behaviour exists. In composite laminates, each calibration coefficient in the calibration matrix is replaced by a 3×3 matrix to consider the elastic constants of the orthotropic plies. Each element of this matrix contains the measured strain of gauge k for a hole of a depth i, when the l component of the residual stress in the range $j\text{-}1 \le i \le j$ is equal to a unit stress. Other researchers have followed this approach for residual stress measurement in composite laminates [13, 14, 16, 19, 27].

In this work the strain gauges are fixed at three known positions. For example, strain gauge *1* is parallel to the fibre direction *x*, strain gauge *3* is in the transverse direction *y* and strain gauge *2* is positioned at 45° (between strain gauges *1* and *3* as in the ASTM type B rosette [26]) or at -135° from strain gauge *1* (for the ASTM type A rosette [26]). Coefficients C_{kl} are calculated for a specific alignment between the strain gauges and the fibres, which needs to be considered during measurement. These calibration coefficients reflect the strains measured at the surface due to the relief of the different residual stresses at each incremental depth of the hole. For example, the presence of a unit stress value σ_x at increment j, contributes to strain values $\varepsilon_1(i)$, $\varepsilon_2(i)$ and $\varepsilon_3(i)$ and the contribution of this unit stress value to the measured strains is given by the coefficients Cij_{11}, Cij_{21} and Cij_{31}, respectively. The same applies for unit stresses σ_y and τ_{xy}. Each matrix C_{kl} in the main compliance matrix C_{ijkl} can be obtained by FEM. Figure 1 summarises the process of obtaining these influence matrices for the case of the ASTM type A rosette and the final compliance matrix C_{ijkl}.

In 2018, Smit and Reid [17] proposed a new approach, extending the power series method initially proposed by Schajer [28] in the 80's. In the new approach, power series are applied separately to each ply orientation instead of being applied to the total hole depth as in Schajer's work. In the original method, due to effects of numerical ill-conditioning, only first order polynomials could be used which reduced its spatial resolution since only linear residual stress distributions could be determined through the total hole depth. The advantage of this method, despite its greater complexity and more difficult practical application, is that errors decrease as the number of the depth increments increases. The integral method behaves inversely due to the error propagation in the inverse problem involved. For this reason, Tikhonov regularization [29] was proposed to approximate the ill-posed problem of the integral method with a well-posed problem to reduce scattering and variance in the final results, while also allowing and even benefiting from the use of an increased number of depth increments [30]. This regularization procedure was adopted in the 2013 revision of the ASTM E837 standard [26] for the case of isotropic materials. As pointed out by Akbari et al. [12], based on the work of Zuccarello [31], the number of the calculation steps should be less than 10 to achieve stable results when the integral method is used without Tikhonov regularization in composite laminates. Attempts have been made to apply Tikhonov regularization to the unit pulse integral method in composite laminates [16, 18]. In such laminates, the released strain at a depth increment is influenced by all components of residual stress in a form that cannot be described analytically at present and the stresses cannot be decoupled, since the relationship between residual stress and released strain does not have a trigonometric form. These facts prevent direct application of Tikhonov regularization to IHD in FML composites, unless the effect of secondary contributions to each strain component is neglected [16, 18]. If the configuration of a composite laminate, as in the case of the samples used in the

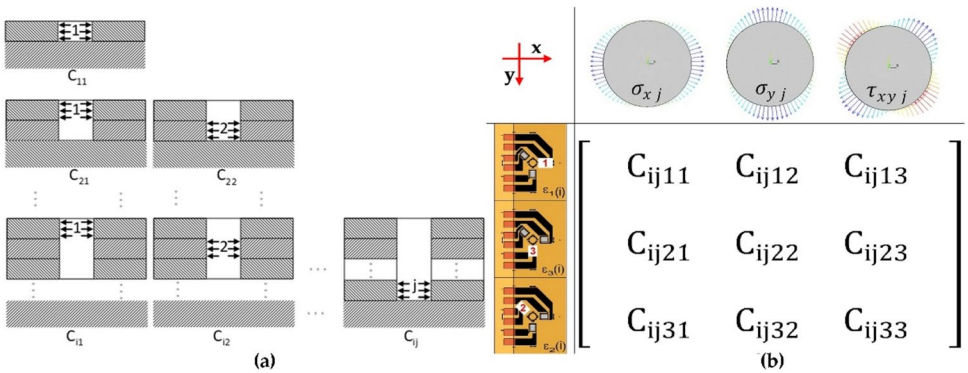

Fig. 1 (**a**) Construction of the compliance matrix C_{ijkl}. (**b**) Strategy to determine the compliance matrix elements C_{kl} based on the unit stresses $\sigma_x = 1$ MPa and $\sigma_y = \tau_{xy} = 0$; $\sigma_y = 1$ MPa and $\sigma_x = \tau_{xy} = 0$; $\tau_{xy} = 1$ MPa and $\sigma_x = \sigma_y = 0$

present work, results in diagonal coefficients of each 3×3 matrix in equation (1) that are dominant due to Poisson's effects, strain and stress in the x direction can be related by:

$$\boldsymbol{\varepsilon_x} = \boldsymbol{C_x}\cdot\boldsymbol{\sigma_x} \Leftrightarrow \varepsilon_x(i) = \sum_{j=1}^{i} C_{ijxx}\cdot\sigma_{jx}. \tag{2}$$

Similar equations can be found for strain and stress components in y and xy directions. Regularization must be adapted to account for the discontinuities at the interfaces between material types. The rows of the regularization operator, L, on both sides of an interface must be set to zero. This ensures that no regularization is applied across the interface between material types [32]. Tikhonov second-derivative regularization can then be implemented separately for each stress component. For example, for the x component:

$$\left(\boldsymbol{C_x^T C_x} + \boldsymbol{\alpha_x L^T L}\right)\boldsymbol{\sigma_x} = \boldsymbol{C_x^T \varepsilon_x}, \tag{3}$$

where α is the regularization parameter that controls the degree of regularization applied. Similar equations can be written for the other components.

The quality of the calculated stress distribution can be significantly affected by the degree of regularization, which can be optimised through the Morozov Discrepancy Principle [33] to maximally remove noise effects without distorting the residual stress distribution. The required value of α can be found iteratively by making the chi-squared statistic, $_x^2$, equal to the number of depth increments. Each ply must be treated separately because the estimated standard error, e, varies between plies. The average local misfit norm [34] is used to estimate the standard strain error separately in each ply. This ensures that smooth stress variations exist within each ply and that deviations from the smooth variation are a result of the measurement noise [35]. The local misfit norm must exclude the misfit across interfaces between plies of different material properties because the released strain at these interfaces can be discontinuous in slope. This ensures that the standard error due to slope discontinuities is not over-estimated, thereby avoiding distortion of the stress results through excessive regularization. The chi-squared statistics when there are n plies with x increments per ply can be determined by [16, 34]:

$$\chi^2 = \sum_{i=1}^{x}\left(\frac{\varepsilon_i^{calc}-\varepsilon_i^{meas}}{e_{ply1}}\right)^2 + \sum_{i=x+1}^{2x}\left(\frac{\varepsilon_i^{calc}-\varepsilon_i^{meas}}{e_{ply2}}\right)^2 + \cdots + \sum_{i=x(n-1)+1}^{nx}\left(\frac{\varepsilon_i^{calc}-\varepsilon_i^{meas}}{e_{plyn}}\right)^2, \tag{4}$$

where ε_i^{meas} is the measured strain and ε_i^{calc} is the regularized fit to the strain data that can be calculated using equation (2).

Considering that each ply has $x \geq 4$ increments per layer, the standard error in each ply, e_{plyi}, can be estimated by [34]:

$$e_{plyi}^2 \approx \sum_{i=1}^{x-3}\left(\frac{\varepsilon_i - 3\varepsilon_{i+1} + 3\varepsilon_{i+2} - \varepsilon_{i+3}}{20(x-3)}\right)^2. \tag{5}$$

After applying Tikhonov regularization to each stress component, the calculated regularized strain fit in each experimental measurement direction can be combined into a full strain vector, ε^{calc}, in the form of equation (1). Equation (1) with the fully coupled calibration matrix, C, and the regularized strain vector, ε^{calc}, is then used to calculate the regularized residual stress distribution. The regularization parameters may require adjustment if the stress solution shows signs of unstable behaviour or distortion.

Smit et al. [16] performed a comparison between the calculation methods referred to above in cross-ply GFRP-steel samples, as used in this work, using neutron diffraction (ND) to evaluate the residual stresses in the metallic layers. Their results showed a good agreement between IHD and ND in the metallic layers. However, the residual stresses determined in the fibre reinforced plies were not experimentally validated. The present work was developed to achieve this goal.

Materials and Methods

Fibre-Metal Laminate Samples

Symmetric laminates with a GFRP/Steel/GFRP lay-up were used in this work. The glass fibres used in the samples were G U300-0/NF-E506/26% type (with 26% resin content), and HC340LA micro-alloyed sheets of steel. The samples were manufactured using an advanced intrinsic manufacturing technology, in which the fibre compound and core metal layer were bonded during the formation of the fibre reinforced polymer. More specifically, a prepared glass fibre prepreg comprising two plies (with a stacking sequence of [0°/90°]) were placed in a heated die of dimensions 25 mm × 250 mm × 100 mm. A metal sheet, with sand blasted surfaces (to enhance bonding behaviour) was placed on the prepreg, and GFRP with a [90°/0°] stacking completed the symmetric stacking as shown in Fig. 2. A punch heated to 160 °C was used to apply a pressure of 0.3 MPa to the laminate. The curing process occurred, at atmospheric conditions, for a period of 18 min. The adhesive bond was simultaneously created within the GFRP itself (between the matrix and fibres) and between the GFRP layers and the metal sheet layer.

The mechanical properties of the samples were obtained according to DIN EN ISO 527, DIN 256 EN ISO 14129 and

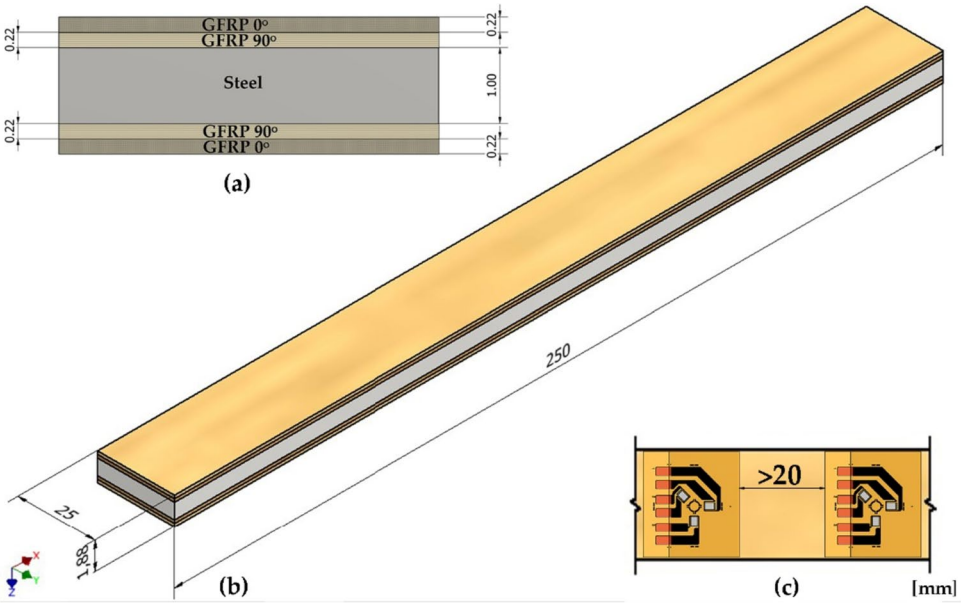

Fig. 2 Fibre-metal laminate sample. (**a**) Stacking ply configuration; (**b**) sample dimensions; (**c**) ASTM E837 type A strain-gauge rosette [26] applied on the surface of the samples

DIN EN ISO 6892-1 as already detailed in previous work [36]. Table 1 presents the mechanical properties determined for the GFRP plies and steel core of the hybrid composite used in the present work.

Experimental Procedure and the HENM Method

The first studies on induced drilling stresses during the application of the hole-drilling technique were performed in metallic materials, where suitable thermal treatments can be applied to relieve residual stresses to achieve an initial "stress-free" state. Beaney and Procter [37] introduced the air abrasion technique for "stress-free" hole-drilling. This "stress-free" state was roughly estimated by Flaman and Herring [38] for different metals and alloys. Previously, Flaman had proposed the use of a pressurized air turbine for ultra-high-speed milling (up to ~ 400,000 rpm), for a "stress-free" application of the hole-drilling technique to metals and their alloys [39]. Nowadays, all commercial equipment for the hole-drilling technique uses Flaman's drilling procedure. Approaches to study induced drilling stresses during hole-drilling were investigated further by Weng et al. [40] using samples cut by electric discharging machining (EDM). However, all these approaches are essentially qualitative and can only give a rough estimate of induced drilling stresses during IHD. In addition, these approaches cannot be applied in fibre reinforced polymers where possible thermal damage to the matrix and the mismatch in the thermal expansion coefficients of the constituents prohibits their application. A hybrid experimental-numerical method (HENM) was proposed to overcome these difficulties in carbon fibre reinforced polymers [41]. Further studies include the successful application of the method to quantify the effect of the drilling operation in glass fibre reinforced polymers [24].

The HENM method is based on the comparison between the strain relaxation field, measured during incremental hole-drilling on a specimen subjected to a well-known applied tensile load (calibration load), and the strain relaxation field calculated by hole simulation on a semi-infinite plate subjected to the same loading using FEM. More precisely, during incremental hole-drilling a set of curves of strain relaxation as a function of depth, corresponding to a given stress state and possible cutting effects, is obtained. This set of curves can also be obtained considering only the applied tensile load without cutting effects through hole-drilling simulation using FEM. The direct comparison between the experimental and numerical curves allows estimation of the effect of the cutting procedure itself. However, the resulting experimental strain relaxation is the superposition of the applied loading, cutting effects and existing

Table 1 Mechanical properties of the GFRP-steel samples constituents [36]

Material	Yield Stress [MPa]	Young's Modulus [GPa]			Poisson's Ratio			Shear Modulus [GPa]		
		E_x	E_y	E_z	ν_{xy}	ν_{xz}	ν_{yz}	G_{xy}	G_{xz}	G_{yz}
GFRP	-	34	8.8	8.8	0.33	0.33	0.37	5.23	5.23	3.21
Steel	380	210			0.29					

residual stresses in the material, i.e., those existing prior to hole-drilling. Therefore, it is necessary to eliminate the effect of the existing residual stresses. To accomplish this, a differential load is applied instead of an absolute one, as presented in Fig. 3.

In previous works [24, 41], hole-drilling is performed for the minimum applied load F_1. After each depth increment, the strains are recorded, and the sample is loaded up to the maximum load F_2. The strains are recorded again, and the sample unloaded up to the minimum load F_1. This process is repeated for all incremental depths until the total hole depth. In the current work, to minimize possible errors due to the recentring process of the hole and to mitigate the possible influence of cutting effects, hole-drilling was performed twice, i.e., for the minimum and maximum applied loads. Using this differential method, the effect of the existing residual stresses can be cancelled and only the applied load affects the measured strain relaxation. Thus, the strain relaxation vs. depth obtained experimentally for the calibration load ΔF (related to $\Delta\sigma$) during incremental hole-drilling can be used as input for the unit pulse integral method, which returns the stresses in the composite laminate due to the calibration load. Considering all experimental data, the finite element method is further used to simulate the hole-drilling in a sample subjected to the same external load ΔF ($\Delta\sigma$). The strain relaxation vs. depth obtained numerically can also be used as input for the unit pulse integral method. When an external tensile load is applied to a composite laminate, uniform stress distributions exist in each ply, with discontinuities at interfaces. Classical lamination theory can be used to analytically determine the stress distribution through the laminate's plies [22, 23], as explained in next section.

To conduct the experimental evaluation of IHD in samples subjected to well-known tensile loads, a horizontal tensile-test machine (HTTM), depicted in Fig. 4, was designed and built with rigidity as a main design criterion. It was important, amongst many design factors, for the HTTM to be able to accommodate simultaneous use of the SINT Technology MTS3000-Restan IHD hole-drilling machine. The hand driven HTTM can be operated at tensile/compression speeds of approximately 0.1 mm/min, allowing quasi-static tensile conditions to be attained on samples.

Before mounting the samples in the machine, a set of type A standard strain gauge rosettes (062UL, Vishay Precision Group, Inc.) [26] were bonded on their surfaces. A dummy rosette was always used for temperature compensation. All strain gauges were connected in a 1/4. Wheatstone bridge circuit to a data acquisition system (HBM Quantum X) with sixteen channels. Three channels were used for IHD measurements, three for temperature compensation and an additional one to connect the precision load cell (HBM S9M). In the present study, two differential loads equal to 700 N and 3500 N were selected. The first calibration load is based on a minimum and maximum load of 500 N and 1200 N, respectively, and the second based on 500 N and 4000 N, respectively. It should be noted that initial residual stresses in the samples were determined in a previous study by IHD and neutron diffraction [16]. The greatest residual stresses (approximately 150 MPa and 200 MPa in the longitudinal and transverse directions of the samples, respectively) were compressive and were determined inside the steel layer near the interface with the 90° ply. In the steel layer, a maximum tensile residual stress of slightly greater than 50 MPa was determined at a depth greater than 0.8 mm, where the uncertainty from IHD is already high. Additionally, CLT predicts a maximum tensile stress of 146 MPa in the steel layer when the tensile load of 4000 N is applied. Therefore, there was no

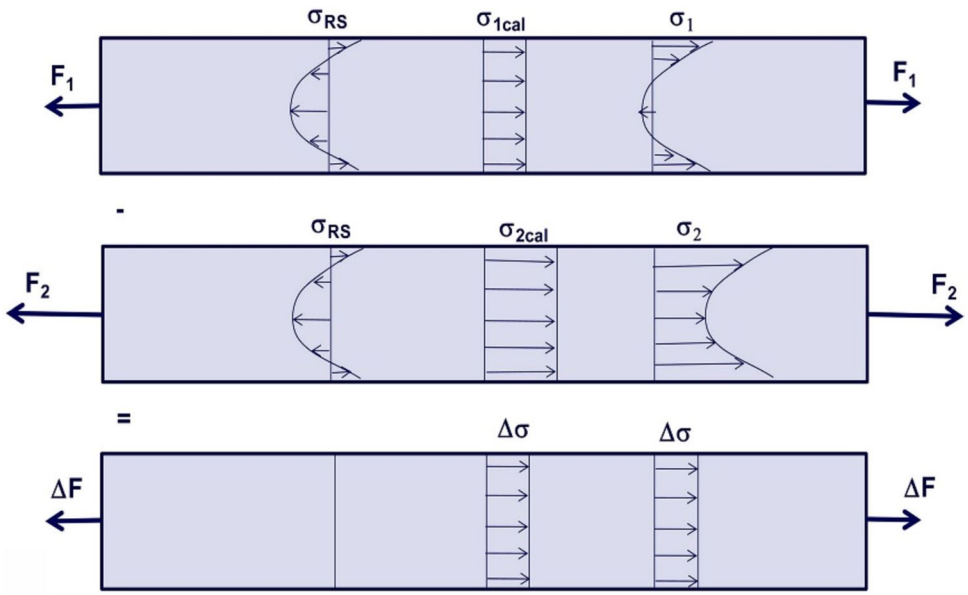

Fig. 3 Principle of superposition used in the proposed method. σ_{RS} is the existing residual stress, σ_{1cal} and σ_{2cal} are stresses resulting from the applied load F_1 and F_2, ΔF and $\Delta\sigma$ are the calibration load and stress

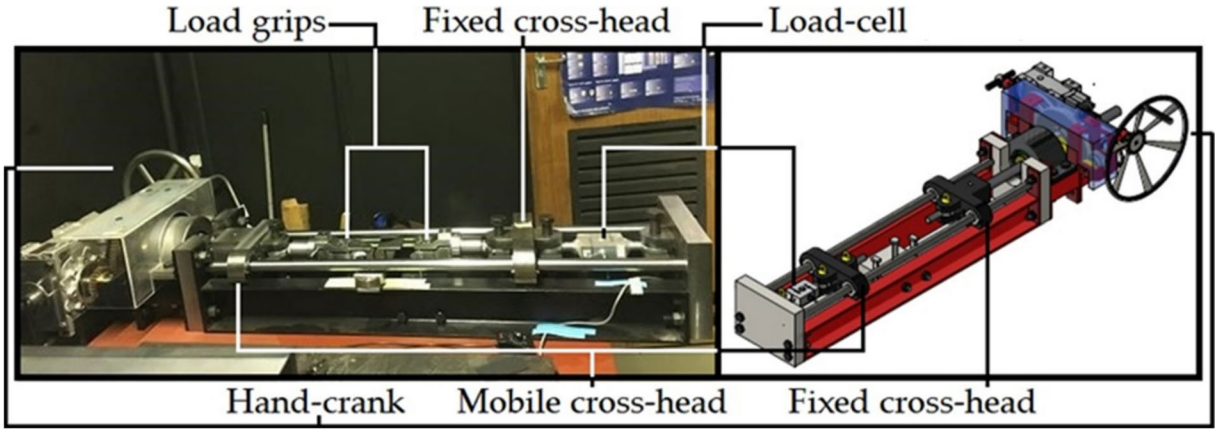

Fig. 4 Horizontal tensile-test machine used in the experimental calibration tests. The samples had a span length of approximately 160 mm

plastic deformation in the steel layer during the tensile tests. The preliminary tests also showed full recovery of strain when the maximum tensile load was removed. Even when considering the stress concentration induced by the hole during IHD, the maximum stress is below 60% of the steel's yield stress and no plasticity effects on IHD results would occur in the steel layer [42] (the ASTM E837 standard suggests a limit of 80% for uniform stresses [26]). However, the stress induced by the greatest load is likely to produce transverse cracking in the 90° plies of the GFRP laminate, since the residual stress transverse to the fibers in the GFRP plies already exceeds 50 MPa in tension. IHD was performed in the tensile samples using depth increments of 10 µm, to reduce drilling induced heating effects in the GFRP plies and to improve accuracy of polynomial interpolation, up to 1 mm depth. Polynomial interpolation was used to fit and smooth strain relaxation data, and the stress evaluation was performed considering four increments per GFRP ply, which correspond to 55 µm incremental depths. In all tests, a feed rate lower than 0.2 mm/min and a time delay greater than 25 s were used. At least three hole combinations for F_1 and F_2 were performed in each sample for a total of six cases for F_1 and F_2, respectively.

Classical Lamination Theory (CLT)

CLT was used to predict the theoretical stress variation across the thickness of each layer of the FML sample while subjected to traction, considering the orthotropy of its plies. Stress $[\sigma]_\theta$ remains uniform across each layer θ and relates to the mid-plane strain $[\varepsilon]_0$ through the lamina stiffness matrix $[\overline{Q}]$ as shown in equation (6) [22]. The lamina stiffness matrix $\overline{Q_{ij}}$ components of each ply (and θ fibre direction) are evaluated from the reduced stiffness matrix Q_{ij} components through a series of equation (7) [22]. Note that in the position (3,3), the subscripts (6,6) are related to the constitutive equation for an orthotropic material obtained from an anisotropic one. In addition, $\overline{Q_{16}}$ and $\overline{Q_{26}}$ are zero for the current samples, since extension-shear coupling is not present in laminae loaded at angles of 0° and 90° relative to the fibre direction.

$$\begin{bmatrix} \sigma_x \\ \sigma_y \\ \tau_{xy} \end{bmatrix}_\theta = \begin{bmatrix} \overline{Q_{11}} & \overline{Q_{12}} & 0 \\ \overline{Q_{21}} & \overline{Q_{22}} & 0 \\ 0 & 0 & \overline{Q_{66}} \end{bmatrix} \cdot \begin{bmatrix} \varepsilon_x \\ \varepsilon_y \\ \gamma_{xy} \end{bmatrix}_0 \tag{6}$$

where:

$$\begin{cases} \overline{Q_{11}} = Q_{11}\cos^4\theta + 2\left(Q_{12}+2Q_{66}\right)\cos^2\theta\sin^2\theta + Q_{22}\sin^4\theta \\ \overline{Q_{12}} = \left(Q_{11}+Q_{22}-4Q_{66}\right)\cos^2\theta\sin^2\theta + Q_{12}\left(\cos^4\theta + \sin^4\theta\right) \\ \overline{Q_{22}} = Q_{11}\sin^4\theta + 2\left(Q_{12}+2Q_{66}\right)\cos^2\theta\sin^2\theta + Q_{22}\cos^4\theta \\ \overline{Q_{66}} = \left(Q_{11}+Q_{22}-2Q_{12}-2Q_{66}\right)\cos^2\theta\sin^2\theta + Q_{66}\left(\cos^4\theta + \sin^4\theta\right) \end{cases} \tag{7}$$

The reduced stiffness matrix components Q_{ij} at each ply are directly dependent on the material properties: elastic moduli (E_1, E_2 and G_{12}) and Poisson's ratios (v_{12} and v_{21}), as can be determined from equation (8) [22, 23].

$$\begin{cases} Q_{11} = \frac{E_1}{1-v_{12}v_{21}} \\ Q_{22} = \frac{E_2}{1-v_{12}v_{21}} \\ Q_{12} = Q_{21} = \frac{v_{12}E_2}{1-v_{12}v_{21}} = \frac{v_{21}E_1}{1-v_{12}v_{21}} \\ Q_{66} = G_{12} \end{cases} \tag{8}$$

In the case of symmetric laminates, the mid-plane strain matrix (in equation (6)) relates to the calibration stress resultant N_x and the extensional stiffness matrix $[A]$, for each respective layer thickness t_k, through equations (9–10) [22, 23].

$$A_{ij} = \sum_{k=1}^{n} \left[\overline{Q_{ij}}\right]_k \cdot t_k \tag{9}$$

and.

$$\begin{bmatrix} N_x \\ N_y \\ N_{xy} \end{bmatrix} = \begin{bmatrix} A_{11} & A_{12} & 0 \\ A_{21} & A_{22} & 0 \\ 0 & 0 & A_{66} \end{bmatrix} \cdot \begin{bmatrix} \varepsilon_x \\ \varepsilon_y \\ \gamma_{xy} \end{bmatrix}_0 \quad (10)$$

Inverting equation (10), the mid-plane strains ε_{ij}^0 can be determined and stresses through the plies can be evaluated from equation (6). If necessary, stress–strain transformation equations can be used to determine the stresses according to the principal material coordinate system.

Numerical Simulation

Numerical simulation was performed using two finite element models. For both cases, APDL scripts were developed for ANSYS Mechanical finite element analysis software. Higher order 3-D 20-node solid elements (SOLID186) [43] that exhibit quadratic displacement behaviour, were used to model the different material layers. These elements are defined by 20 nodes having three degrees of freedom per node: translations in the nodal x, y, and z directions. These elements were used with two available key options in ANSYS; the layered structural solid option to model the layered thick shells, which allow modelling of the different glass fibre plies, and the homogeneous structural solid option to model the metallic (steel) core.

The first model was developed to determine the calibration coefficients that relate the relieved strains to the stresses present in the material and can be easily modified for a given composite laminate. Nine elastic constants (E_x, E_y, E_z, ν_{xy}, ν_{xz}, ν_{yz}, G_{xy}, G_{xz}, G_{yz}) are required to relate the stresses and strains in an orthotropic and layered material – see Table 1. To determine the whole compliance C_{ijkl} matrix, according to the description provided previously (see Fig. 1), a full 3D cylindrical model with an external diameter equal to 5 times the average radius of the strain gauge rosette (to avoid edge effects) was used. Figure 5(a) shows the FEM mesh used in this case with the constraints applied only on the outer diameter of the model and Fig. 5(b) shows an enlarged view of the mesh near the hole, showing the position of the strain gauge grids of the ASTM type A rosette used (Fig. 5(c)). Only the nodes at outer diameter, as shown in Fig. 5(a), were constrained to avoid free body motion. Since, in this case, the thickness can be considered a sensitive parameter in FE analysis, as previously observed [44, 45], the model should only be constrained far from the hole position to avoid boundary effects.

For obtaining the whole compliance C_{ijkl} matrix, the effects of σ_x, σ_y and τ_{xy} on the strain, ε_k, measured by each gauge of the rosette, are considered separately. All matrix values can be determined considering three different unit stress states, as shown in Fig. 1(b). As stated before, the presence of a unit stress value $\sigma_x = 1$ and $\sigma_y = \tau_{xy} = 0$, at increment j, contributes to strain values $\varepsilon_1(i)$, $\varepsilon_2(i)$ and $\varepsilon_3(i)$ and the contribution of this unit stress value to the measured strains is given by the coefficients Cij_{11}, Cij_{21} and Cij_{31}, respectively, for the first column. The second column, considering $\sigma_y = 1$, $\sigma_x = \tau_{xy} = 0$, and the last column considering a pure shear stress state $\tau_{xy} = 1$, $\sigma_x = \sigma_y = 0$. The unit loads are converted into the cylindrical coordinate system by equation (11) [14], and σ_r and $\tau_{r\theta}$ are applied at the hole boundary, within each depth increment, using the SURF154 3-D structural surface effect element [43].

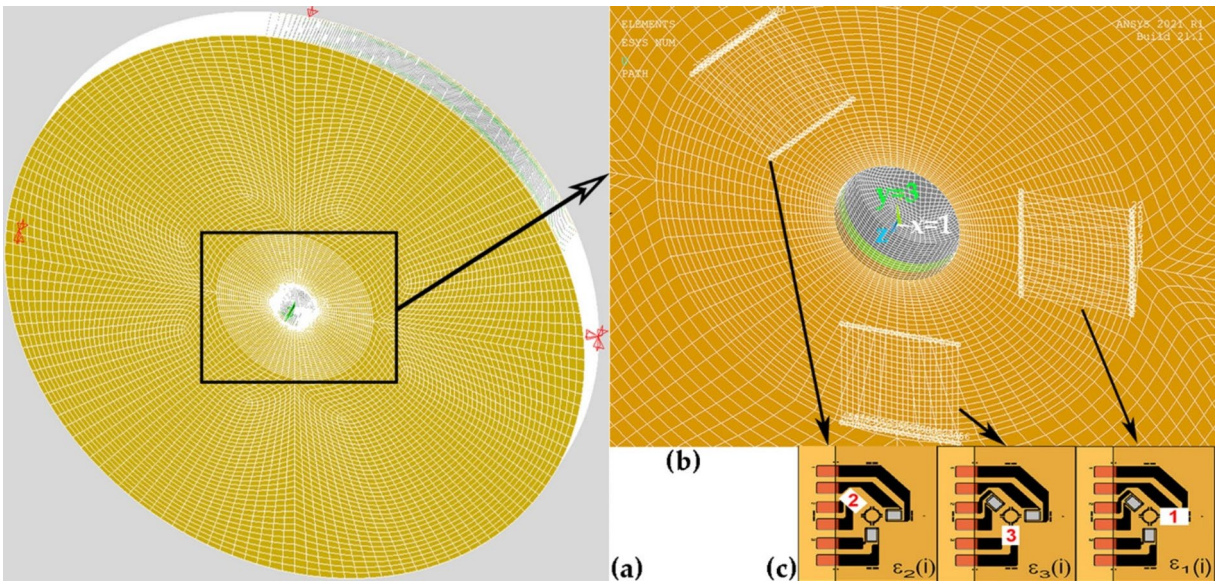

Fig. 5 (**a**) 3D-FEM mesh for the determination of calibration coefficients matrix C_{ijkl}. (**b**) Enlarged view near the hole (1 mm depth), showing the strain gauge grids (1.57 mm length) of the (**c**) 3-element ASTM type A rosette used (062UL, Vishay Precision Group, Inc.)

$$\begin{bmatrix} \sigma_r \\ \tau_{r\theta} \end{bmatrix} = \begin{bmatrix} \cos^2\theta & \sin^2\theta & \sin 2\theta \\ -0.5 \cdot \sin 2\theta & 0.5 \cdot \sin 2\theta & \cos 2\theta \end{bmatrix} \cdot \begin{bmatrix} \sigma_x \\ \sigma_y \\ \tau_{xy} \end{bmatrix} \quad (11)$$

A second model was developed for the hole-drilling simulation in the samples subjected to a given applied uniaxial tensile load, as per the HENM method – see Fig. 3. To determine the strain-depth relaxation curves when the samples are subjected to a given tensile calibration load (in the present study 700 N and 3500 N, respectively), considering the existing symmetries, a ¼ 3D plate model was used as shown in Fig. 6(a). Strain gauge grids are also shown in Fig. 6(b). The superposition of the grids here is apparent, because strain gauge 2 is artificially placed in the first quadrant. As for the other model, it was only constrained at the basal nodes of the external boundary of the plate to prevent rigid body motion. Both models have the same mesh configuration and refinement within a radius that extends to the outer edges of the gauges.

A total sample thickness of 1.88 mm, corresponding to 0.22 mm thickness for each GFRP ply and 1 mm thickness for the internal steel core was considered (as per Fig. 2). A mean hole diameter of 1.8 mm, as observed during the experimental tests was used. The incremental hole depth simulation was performed using the "birth and death of elements" ANSYS code features, considering four depth increments per GFRP ply (55 μm each) and a further ten increments in the steel core, for a total of eighteen depth increments up to a depth of roughly 1 mm. After each depth increment, the nodal displacement values were integrated over an area equivalent to the strain gauge grids, following a procedure proposed by Schajer [46].

Results and Discussion

First, it was necessary to verify the linear elastic hypothesis between the applied load and the measured strains during the tensile tests. Figure 7(a) shows the evolution of the measured strain in the longitudinal direction of the sample with the applied tensile load, during loading and unloading. A linear relationship between the applied load and the strain measured is observed. A coefficient of determination R squared near 1 was determined and, therefore, the hypothesis is satisfied.

Thus, considering the CLT theory for an applied tensile load of 700 N and a 25 mm wide sample, an $N_x = 28$ N/mm force resultant is obtained and used to evaluate the stresses in each ply through equation (6). For this loading ($N_y = N_{xy} = 0$), the distribution of the longitudinal stress through the plies of the laminate can be determined. Longitudinal uniform stresses in each layer (σ_x) of 4.2, 1.0 and 25.7 MPa, respectively, for the GFRP fibre orientation at 0°, 90° and the steel layer are determined for the FML sample shown in Fig. 2. Considering the cross-sectional area of the samples (1.88 mm × 25 mm), a uniform mean stress of 14.9 MPa through the thickness would be expected for the case of an isotropic material. However, since each ply of the laminate presents a different mechanical behaviour, there is a distribution of stress through the plies of the laminate, as predicted by both CLT theory and numerical simulation using FEM, as shown in Fig. 7(b). There is an almost exact match between CLT and FEM results. Note the discontinuity in stress when passing from one ply to another. Similar results are obtained when a tensile load of 3500 N is applied. In this case, longitudinal uniform stresses in each layer (σ_x) of 20.8, 5.0 and

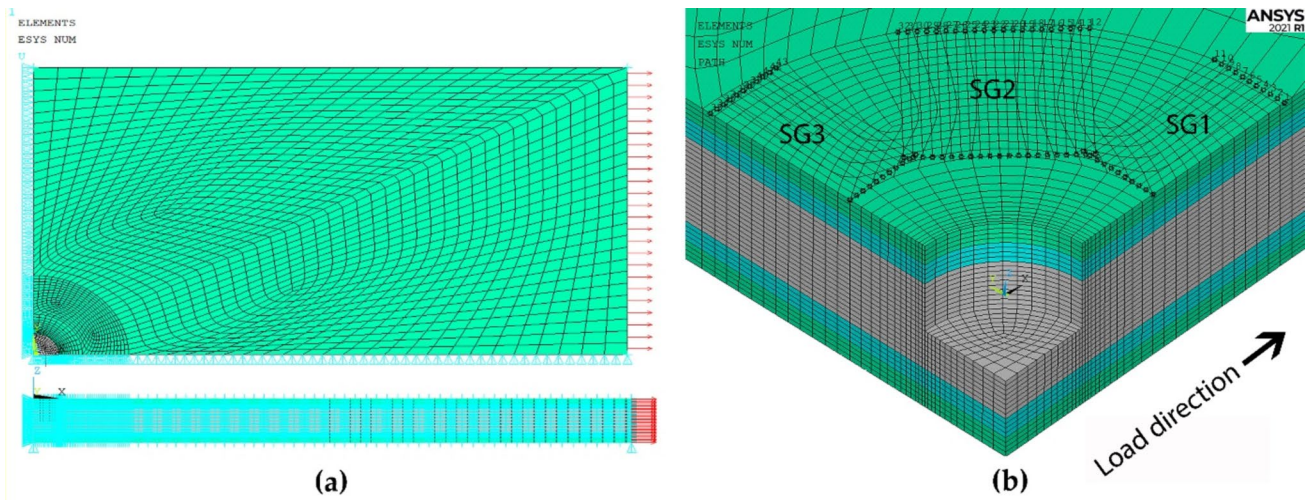

Fig. 6 (**a**) **3D-**FEM mesh for hole-drilling simulation of the GFRP-steel plate subjected to a given tensile load. (**b**) Enlarged view near the hole (1 mm depth), showing the strain gauge grids (1.57 mm length) (ASTM type A - 062UL, Vishay Precision Group, Inc.)

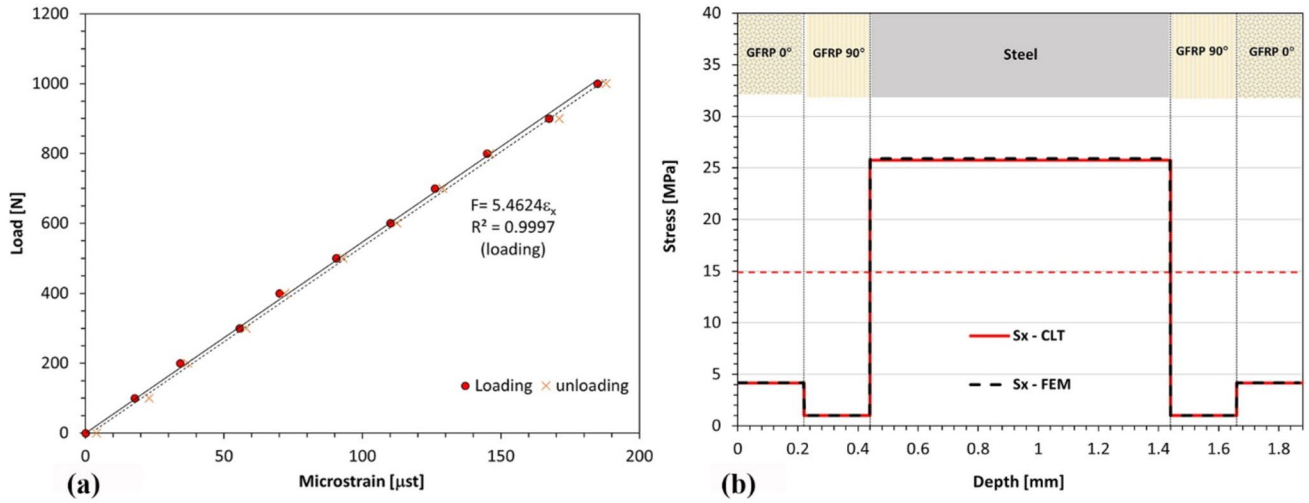

Fig. 7 (**a**) Applied axial load vs. measured strain in the longitudinal direction of the samples (in x direction as per Fig. 2). (**b**) Longitudinal stress (x) arising in each laminate's ply for a tensile load of 700 N, according to CLT and numerical simulation using FEM

128.6 MPa, respectively, for the GFRP fibre orientation at 0°, 90° and the steel layer are determined. However, for the 3500 N load, transverse cracking is likely to occur at layers with the fibres oriented at 90° to the direction of the tensile load due to the stress concentration induced by the hole and the initial residual stresses within the FML. The main research question is whether the IHD technique can accurately determine such stress distributions.

As explained previously, the experimental IHD is performed when the samples are subjected to a minimum and maximum load. These minima and maxima led to a calibration load of 700 N and 3500 N, respectively. The resultant strain relaxation curve versus depth for each tensile load can be seen in Fig. 8. Uncertainty analysis was performed considering the total number of tests carried out and the standard deviation is included for the average strain relaxation observed in each incremental depth. As expected, maximum values are observed at strain gauge 1 which is oriented with the longitudinal direction of the samples and coincides with the direction of the applied load. In the transverse direction, strain measurement in strain gauge 3 is only due to Poisson's effects.

In Fig. 8(a), a variation in slope is observed in the strain relaxation curves when passing from one layer to another. For the 3500 N load in Fig. 8(b), this variation is not evident. In both Figs., dotted lines correspond to the best polynomial fit to the relieved strain in each ply. This interpolation is necessary to determine the strain relaxation when different numbers of depth increments per ply are considered. These curves ($\varepsilon_i^{exp}(z)$) will be further used as input for the integral method for residual stress calculation by IHD.

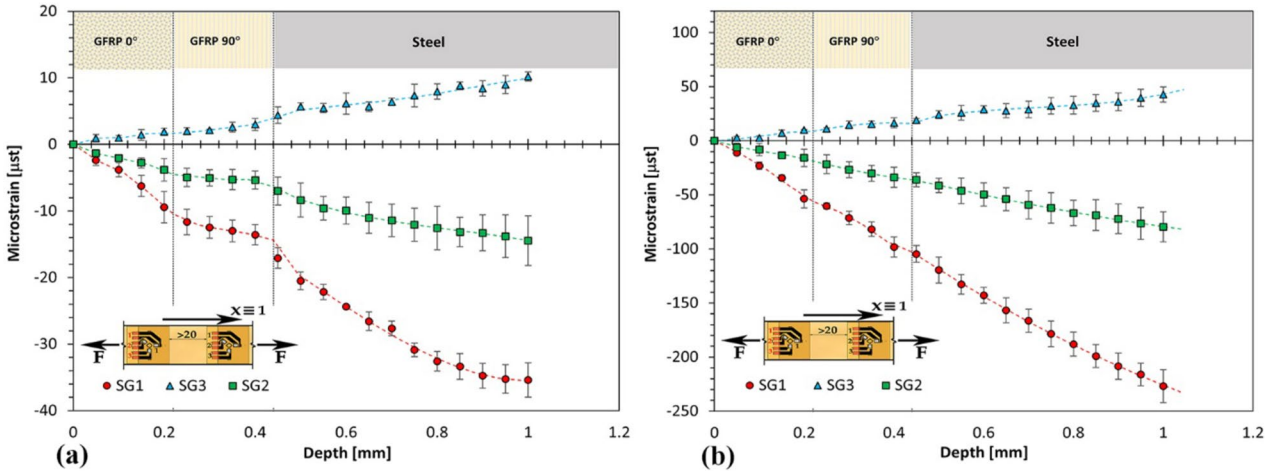

Fig. 8 Experimental strain relaxation vs. hole depth. (**a**) Tensile load of 700 N and (**b**) 3500 N

Considering the FEM simulation of the incremental hole-drilling, based on the data obtained during the experimental tests, a set of numerical curves ($\varepsilon_i^{num}(z)$) can also be determined, which can be superimposed on the experimental ones. Figure 9 shows the obtained results. Some observations should be pointed out. Hole-drilling simulation by FEM, assuming the material behaves linearly and elastically, presents strain-depth relaxation curves with the same trend for both applied loads, regardless of the difference in the magnitude of the measured strain relief. As seen in Fig. 9(a), for the lowest applied load of 700 N, there is a good agreement between the experimental and numerical results in all glass fibre layers, but a slight deviation in the steel layer. The most important results are those in the direction of the strain gauge 1 which is oriented with the direction of the tensile load. The stresses calculated from these curves for IHD are more related with their slopes than with their absolute values. For the 3500 N load, as shown in Fig. 9(b), there is only a good agreement in the first ply, corresponding to the layer with the fibres oriented at 0° (GFRP 0°). The divergence between the experimental and numerical results observed in the second ply (GFRP 90°) is probably a result of the appearance of transverse cracking or delamination occurring in this layer. To attain the calibration load of 3500 N, a maximum load of 4000 N was applied to the samples. This high applied load, together with the stress concentration induced by the hole and the existing tensile residual stresses, as determined in previous work [16], has a high probability of having caused transverse cracking or delamination and consequently having increased the measured strain relaxation. Similar concerns have been expressed in previous work [16]. This effect can explain the divergence observed in the experimental strain relaxation values compared to the numerical ones at this load.

The experimental, $\varepsilon_i^{exp}(z)$, and numerical, $\varepsilon_i^{num}(z)$, strain-depth relaxation curves can be used together with the calibration coefficients matrix, C_{ijkl}, determined by FEM, to evaluate the stress distribution in the FML samples via IHD. Equation (1) or equation (3), for using the unit pulse integral method with or without regularization, respectively, can then be used to compute the stress distribution. For the numerical strain-depth relaxation curves no regularization is needed since there is no noise or outliers. For the residual stress calculation by the integral method, strong numerical ill-conditioning effects begin when the total hole depth becomes greater than half of the hole diameter [25]. This behaviour has also been confirmed in GFRP laminates [47]. Therefore, stress calculation is performed up to a hole depth equal to the half of the hole diameter (~ 0,9 mm). Considering four increments per FRP ply and a total of sixteen depth increments, the unit pulse integral method without regularization (equation (1)) was used with experimental and numerical strain-depth relaxation curves. Tikhonov regularization (equation (3)) was only used with the experimental strain-depth relaxation curves. Figure 10 shows the results obtained, compared with those determined by CLT.

For both applied loads, IHD numerical results agree very well with the results predicted by CLT in all glass fibre layers. The difference observed in the steel layer (around 3% avg.) could be related to the small numerical differences induced by the fact that two FEM models are used (a full 3D cylindrical model for the determination of C matrix and a ¼ 3D plate for the hole-drilling simulation in the tensile samples). The full 3D cylindrical model developed can be used for any composite laminate subjected to IHD, while the ¼ 3D plate models the samples subjected to tensile loading during the performed experiments only.

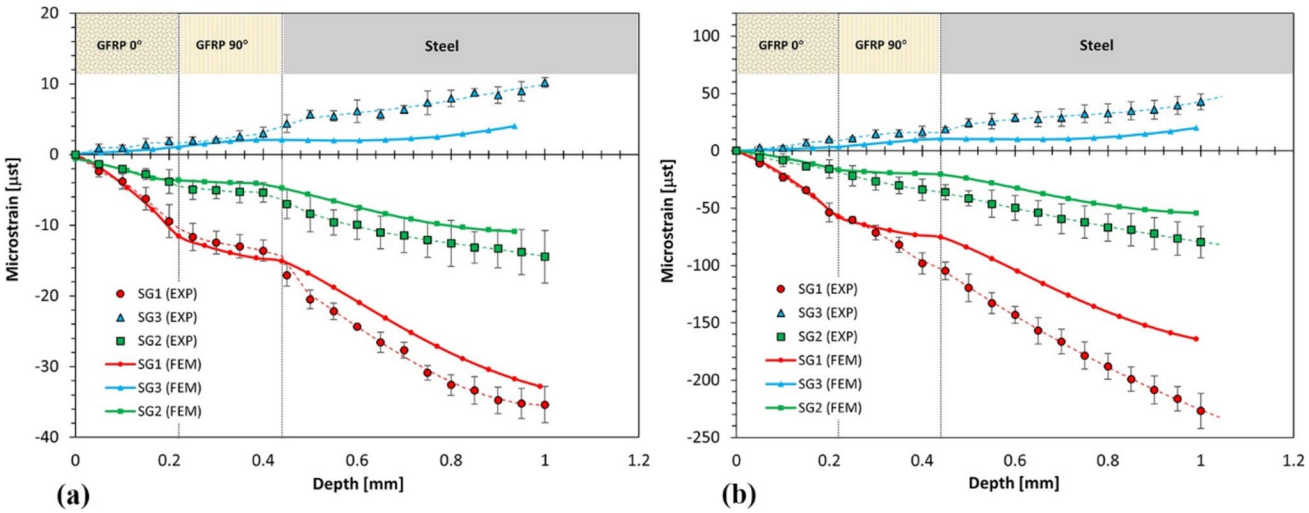

Fig. 9 $\varepsilon_i^{exp}(z)$ vs. $\varepsilon_i^{num}(z)$, where z corresponds to the hole depth. (**a**) Tensile load of 700 N and (**b**) 3500 N

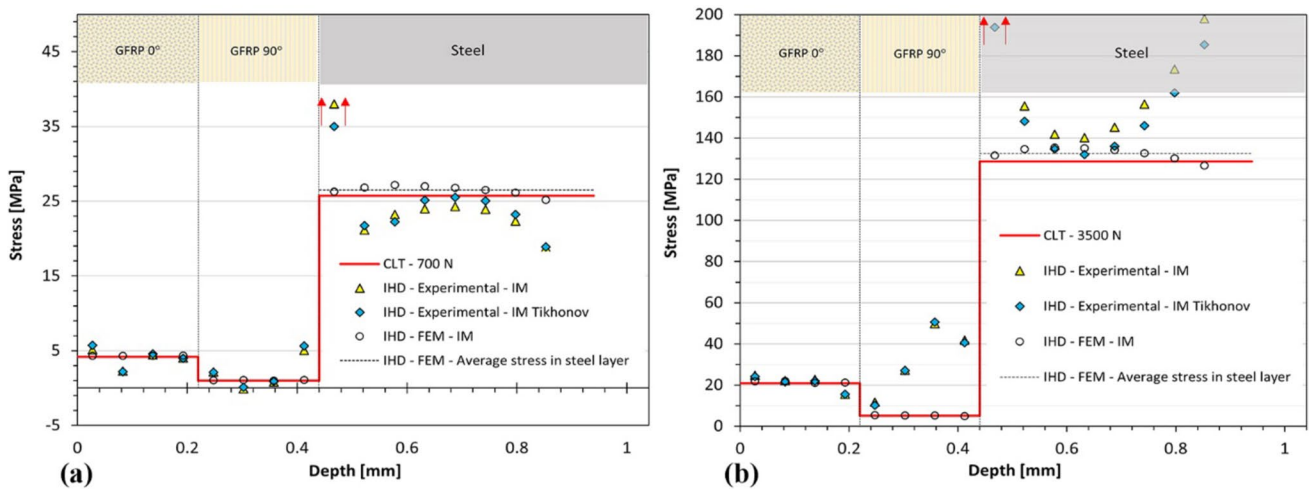

Fig. 10 Stress $\sigma_{xi}^{exp}(z)$ vs. $\sigma_{xi}^{num}(z)$, vs. $\sigma_{xi}^{theor}(z)$. (**a**) Applied load of 700 N and (**b**) 3500 N

For the lowest applied load of 700 N, a good agreement is observed in all GFRP plies, as shown in Fig. 10(a), which corroborates previous observations made by Nobre et al. [24]. The average stress value is near the stress predicted by the CLT theory and IHD numerical results. This is also valid for the first GFRP layer, for the case of the 3500 N applied load. However, for this load, the experimental stress determined by IHD in the 90° layer is not uniform, as predicted by the CLT theory and numerical IHD, but presents an increasing trend through the layer, which is believed to be due to the appearance of transverse cracking or delamination, as previously mentioned. The high strain values in this layer also affect the stress results observed in the steel layer, which are much greater than that predicted by the CLT theory and numerical IHD. For the steel layer and for the 700 N applied load, experimental IHD stress results are much more reliable than those obtained for the 3500 N load, but not uniform as expected and as theoretically and numerically predicted. There is a parabolic stress distribution, instead of a perfectly uniform one. Tikhonov regularization slightly improves the results. The small experimental strain errors in the GFRP layers lead to higher errors in stress at deeper increments corresponding to the steel layer. This relates with the intrinsically high error sensitivity and error propagation of the integral method itself (ill-posed inverse problem). The polynomial interpolation conducted in each layer is less constrained at its ends. Consequently, larger errors are to be expected near the interfaces. At the GFRP-steel interface, this effect, coupled with the high modulus of the steel, results in a large error in the first stress measured within the steel. The stress near the interface in the GFRP is, however, accurately determined by IHD. Additional work should be carried out regarding this issue to improve the accuracy of IHD in the tensile samples, such as using cubic splines for the interpolation of the experimental strain relaxation values and improving the regularization procedures for IHD in composite laminates.

Conclusions

Based on the results of this study, incremental hole-drilling can evaluate the stress distribution in fibre-metal hybrid composites subjected to tensile loading, using commercially available equipment for IHD, provided that the tensile load is low enough to avoid transverse cracking or delamination in the fibre reinforced plies.

Stresses near interfaces, where the stress is discontinuous, were determined with acceptable accuracy in the GFRP layers, whilst at the deeper GFRP-steel interface a discrepancy was observed. The discrepancy near this interface seems to be related with the large stress variation observed at this interface, the uncertainty of the strain relaxation measured during IHD and the polynomial fit needed to describe the experimental strain-depth relaxation curves through the thickness of the composite laminate. Stresses near singularity regions at FRP-metal interface at deeper layers are challenging to be accurately determined, due to the greater uncertainty associated with measured strain relaxation at deeper increments. Nonetheless, IHD seems to be an appropriate measurement technique to provide the necessary information about the residual stresses arising in these regions.

Additional research is needed to extend regularization procedures to these materials for a better assessment of non-uniform residual stresses through the plies of the laminate, particularly near the interfaces at deeper layers. Improving accuracy in measuring strain relief, the use of cubic splines

for fitting the measured strain relaxation through the depth (especially at interface regions) or the use of the separate series expansion method could enable reducing the size of depth increments and, therefore, enhance the determination of residual stresses in these regions.

Acknowledgements Professor T. Tröster and his group at University of Paderborn (Automotive Lightweight Design, (LiA)) are thanked for providing the samples used in this research.

Author Contributions Conceptualization, J.P. Nobre; methodology, J.P. Nobre and T.C. Smit; software, J.P. Nobre, T.C. Smit and T. Wu; validation, J.P. Nobre and T.C. Smit; formal analysis, J.P. Nobre and T.C. Smit; investigation, Q. Qhola, J.P. Nobre and T.C. Smit; resources, T. Niendorf, J.P. Nobre and R. Reid; writing—original draft preparation, J.P Nobre; writing—review and editing, T.C. Smit, R. Reid, T. Wu and T. Niendorf; supervision, T. Niendorf, R. Reid, J.P. Nobre and T.C. Smit; project administration, T. Niendorf, J.P. Nobre and T. Wu; funding acquisition, T. Niendorf and J.P. Nobre. All authors have read and agreed to the published version of the manuscript.

Funding Open access funding provided by FCT|FCCN (b-on). The research leading to these results received funding from German Research Foundation (DFG – Deutsche Forschungsgemeinschaft) under Grant Agreement No 399304816 and from the National Research Foundation of South Africa (NRF) under Grant Agreement No 106036. This work was also supported by funds from FCT – Fundação para a Ciência e a Tecnologia, I.P., within the projects UIDB/04564/2020 and UIDP/04564/2020.

Data Availability All data presented in this manuscript will be available on request.

Declarations

Conflict of Interest The authors declare that they have no conflict of interest.

Statements on Human and Animal Rights Not applicable.

Informed Consent Not applicable.

References

1. Sinmazçelik T, Avcu E, Bora MÖ, Çoban O (2011) A review: Fibre metal laminates, background, bonding types and applied test methods. Mater Des 32(7):3671–3685. https://doi.org/10.1016/j.matdes.2011.03.011
2. Vlot A, Gunnink JW (2001) Fibre Metal laminates. Springer Neth. https://doi.org/10.1007/978-94-010-0995-9
3. Wittenberg TC, van Baten TJ, de Boer A (2001) Design of fiber metal laminate shear panels for ultra-high capacity aircraft. Aircr Des 4(2):99–113. https://doi.org/10.1016/S1369-8869(01)00003-9
4. Ding Z, Wang H, Luo J, Li N (2021) A review on forming technologies of fibre metal laminates. Int J Lightweight Mater Manuf 4(1):110–126. https://doi.org/10.1016/j.ijlmm.2020.06.006
5. Prussak R, Stefaniak D, Hühne C, Sinapius M (2018) Evaluation of residual stress development in FRP-metal hybrids using fiber Bragg grating sensors. Prod Eng Res Devel 12(2):259–267. https://doi.org/10.1007/s11740-018-0793-4
6. Scholtes B (1991) Eigenspannungen in mechanischen randschichtverformten Werkstoffzuständen: Ursachen, Ermittlung und Bewertung. DGM Informationsgesellschaft, Oberursel
7. Parlevliet PP, Bersee HEN, Beukers A (2007) Residual stresses in thermoplastic composites – a study of the literature. Part III: effects of thermal residual stresses. Compos Part A Appl Sci Manufac 38(6):1581–1596. https://doi.org/10.1016/j.compositesa.2006.12.005
8. Awaja F, Zhang S, Tripathi M, Nikiforov A, Pugno N (2016) Cracks, microcracks and fracture in polymer structures: formation, detection, autonomic repair. Prog Mater Sci 83:536–573. https://doi.org/10.1016/j.pmatsci.2016.07.007
9. Hiemstra DL, Sottos NR (1993) Thermally induced interfacial microcracking in polymer matrix composites. J Compos Mater 27(10):1030–1051. https://doi.org/10.1177/002199839302701005
10. Hausmann J, Naghipour P, Schulze K (2013) Analytical and numerical residual stress models for fiber metal laminates – comparison and application. Procedia Mater Sci 2:68–73. https://doi.org/10.1016/j.mspro.2013.02.009
11. Vu QT, Seon G, Ghaffari S, Makeev A, Lachaud F, Charlotte M, Gourinat Y (2023) Evaluating Residual Stress in Carbon Fiber-Reinforced Polymer (CFRP) at Microscale Using Fiber Push-Out Experiment and Finite Element Modeling. Polymers. https://doi.org/10.3390/polym15122596
12. Akbari S, Taheri-Behrooz F, Shokrieh MM (2014) Characterization of residual stresses in a thin-walled filament wound carbon/epoxy ring using incremental hole drilling method. Compos Sci Technol 94:8–15. https://doi.org/10.1016/j.compscitech.2014.01.008
13. Ghasemi AR, Mohammadi MM (2016) Residual stress measurement of fiber metal laminates using incremental hole-drilling technique in consideration of the integral method. Int J Mech Sci 114:246–256. https://doi.org/10.1016/j.ijmecsci.2016.05.025
14. Magnier A, Wu T, Tinkloh SR, Tröster T, Scholtes B, Niendorf T (2021) On the reliability of residual stress measurements in unidirectional carbon fibre reinforced epoxy composites. Polym Test 97:107146. https://doi.org/10.1016/j.polymertesting.2021.107146
15. Schajer GS, Yang L (1994) Residual-stress measurement in orthotropic materials using the hole-drilling method. Exp Mech 34(4):324–333. https://doi.org/10.1007/BF02325147
16. Smit TC, Nobre JP, Reid RG, Wu T, Niendorf T, Marais D, Venter AM (2022) Assessment and Validation of Incremental Hole-Drilling Calculation Methods for Residual Stress Determination in Fiber-Metal Laminates. Exp Mech 62(8):1289–1304. https://doi.org/10.1007/s11340-022-00848-4
17. Smit TC, Reid RG (2018) Residual stress measurement in composite laminates using incremental hole-drilling with power series. Exp Mech 58(8):1221–1235. https://doi.org/10.1007/s11340-018-0403-6
18. Smit TC, Reid RG (2020) Tikhonov regularization with incremental hole-drilling and the integral method in cross-ply composite laminates. Exp Mech 60(8):1135–1148. https://doi.org/10.1007/s11340-020-00629-x
19. Wu T, Tinkloh SR, Tröster T, Zinn W, Niendorf T (2020) Determination and validation of residual stresses in CFRP/metal hybrid

components using the incremental hole drilling method. J Compos Sci 4(3):143. https://doi.org/10.3390/jcs4030143
20. Nau A, Scholtes B, Rohleder M, Nobre JP (2011) Application of the hole drilling method for residual stress analyses in components made of polycarbonate. Zeitschrift Kunststofftechnik (WAK). Carl Hanser Verlag 7(3):66–85
21. Liu G, Tang K (2015) Study on stress concentration in notched cross-ply laminates under tensile loading. J Compos Mater 50(3):283–296. https://doi.org/10.1177/0021998315573802
22. Hyer MW (2009) Stress analysis of fiber-reinforced composite materials. DEStech Publications, Inc, Lancaster, PA, USA
23. Nettles AT (1994) Basic Mechanics of Laminated Composite Plates. NASA Reference Publication 1351 (NASA-RP-1351), Marshall Space Flight Center, Huntsville, AL, USA
24. Nobre JP, Stiffel JH, Nau A, Outeiro JC, Batista AC, Van Paepegem W, Scholtes B (2013) Induced drilling strains in glass fibre reinforced epoxy composites. CIRP Ann 62(1):87–90. https://doi.org/10.1016/j.cirp.2013.03.089
25. Schajer GS (1988) Measurement of non-uniform residual stress using the hole-drilling method. Part II-Practical application of the integral method. J Eng Mat Tech (ASME) 110(4):344–349. https://doi.org/10.1115/1.3226060
26. ASTM-E837-20 (2020) Standard test method for determining residual stresses by the hole-drilling strain-gage method. ASTM International, West Conshohocken, PA, wwwastmorg
27. Liu X, Wang X, Guan Z, Jiang T, Geng K, Li Z (2021) Improvement and validation of residual stress measurement in composite laminates using the incremental hole-drilling method. Mech Mater 154:103715. https://doi.org/10.1016/j.mechmat.2020.103715
28. Schajer GS (1981) Application of Finite element calculations to residual stress measurements. J Eng Mater Technol 103:157–163. https://doi.org/10.1115/1.3224988
29. Schajer GS (2007) Hole-drilling residual stress profiling with automated smoothing. J Eng Mater Technol 129(3):440–445. https://doi.org/10.1115/1.2744416
30. Beghini M, Grossi T, Prime MB, Santus C (2023) III-posedness and the bias-variance tradeoff in residual stress measurement inverse solutions. Exp Mech 63(3):495–516. https://doi.org/10.1007/s11340-022-00928-5
31. Zuccarello B (1999) Optimal calculation steps for the evaluation of residual stress by the incremental hole-drilling method. Exp Mech 39(2):117–124. https://doi.org/10.1007/BF02331114
32. Prime MB, Crane DL (2014) Slitting method measurement of residual stress profiles, including stress discontinuities, in layered specimens. In: Rossi M et al. (eds) Residual Stress, Thermomechanics & Infrared Imaging, Hybrid Techniques and Inverse Problems, Volume 8. Conference Proceedings of the Society for Experimental Mechanics Series. Springer, Cham. https://doi.org/10.1007/978-3-319-00876-9_12
33. Tikhonov AN, Goncharsky AV, Stepanov VV, Yagola AG (1995) Numerical methods for the approximate solution of ill-posed problems on compact sets. In: Tikhonov AN, Goncharsky AV, Stepanov VV, Yagola AG (eds) Numerical methods for the solution of Ill-posed problems. Springer Netherlands, Dordrecht, pp 65–79. https://doi.org/10.1007/978-94-015-8480-7_3
34. Schajer G, Prime M (2006) Use of Inverse solutions for residual stress measurement. J Eng Mater Technol 128:375–382. https://doi.org/10.1115/1.2204952
35. Akbari S, Taheri-Behrooz F, Shokrieh MM (2013) Slitting measurement of residual hoop stresses through the wall-thickness of a filament wound composite ring. Exp Mech 53(9):1509–1518. https://doi.org/10.1007/s11340-013-9768-8
36. Wu T, Tinkloh S, Tröster T, Zinn W, Niendorf T (2021) Measurement and analysis of residual stresses and warpage in fiber reinforced plastic and hybrid components. Metals 11(2):335. https://doi.org/10.3390/met11020335
37. Beaney EM, Procter E (1974) A critical evaluation of the centre hole technique for the measurement of residual stresses. Strain 10(1):7–14. https://doi.org/10.1111/j.1475-1305.1974.tb00074.x
38. Flaman MT, Herring JA (2008) Comparison of four hole-producing techniques for the Center-Hole residual-stress measurement method. Exp Tech 9:30–32. https://doi.org/10.1111/j.1747-1567.1985.tb02036.x
39. Flaman MT (1982) Brief investigation of induced drilling stresses in the center-hole method of residual-stress measurement. Exp Mech 22(1):26–30. https://doi.org/10.1007/BF02325700
40. Weng CC, Lin YC, Chou CP (1992) A new approach for determining the induced drilling stresses in the hole-drilling method of residual-stress measurement. Exp Tech 16(5):33–35. https://doi.org/10.1111/j.1747-1567.1992.tb00704.x
41. Nobre JP, Stiffel JH, Paepegem WV, Nau A, Batista AC, Marques MJ, Scholtes B (2011) Quantifying the drilling effect during the application of incremental hole-drilling technique in laminate composites. Mater Sci Forum 681:510–515. https://doi.org/10.4028/www.scientific.net/MSF.681.510
42. Nobre JP, Kornmeier M, Scholtes B (2018) Plasticity effects in the hole-drilling residual stress measurement in peened surfaces. Exp Mech 58:369–380. https://doi.org/10.1007/s11340-017-0352-5
43. ANSYS (2017) Mechanical APDL theory reference. Release 17.1. SAS IP, Inc., Canonsburg. PA, USA
44. Magnier A (2019) Residual stress analysis in polymer materials using the hole drilling method - basic principles and applications. Dissertation, University of Kassel, kup: kassel university press. https://doi.org/10.19211/KUP9783737606455
45. Nobre JP, Polese C, van Staden SN (2020) Incremental hole drilling residual stress measurement in thin aluminum alloy plates subjected to laser shock peening. Exp Mech 60:553–564. https://doi.org/10.1007/s11340-020-00586-5
46. Schajer GS (1993) Use of displacement data to calculate strain gauge response in non-uniform strain fields. Strain 29(1):9–13. https://doi.org/10.1111/j.1475-1305.1993.tb00820.x
47. Reid RG, Smit TC (2023) Evaluation of the maximum allowable hole depth for IHD of GFRP laminates. In: Tighe RC, Considine J, Kramer SL, Berfield T (eds) Thermomechanics & Infrared Imaging, Inverse Problem Methodologies and Mechanics of Additive & Advanced Manufactured Materials, Volume 6. SEM 2022. Conference Proceedings of the Society for Experimental Mechanics Series. Springer, Cham. https://doi.org/10.1007/978-3-031-17475-9_1